

Multiplex core-periphery organization of the human connectome

Federico Battiston^{a,b,c}, Jeremy Guillon^{a,b}, Mario Chavez^b, Vito Latora^{c,d}, Fabrizio De Vico Fallani^{a,b,*}

^a*Inria Paris, Aramis project-team, 75013, Paris, France*

^b*CNRS, Sorbonne Universites, UPMC Univ Paris 06, Inserm, Institut du cerveau et la moelle epiniere (ICM), Hopital Pitie-Salpetriere, 75013, Paris, France*

^c*School of Mathematical Sciences, Queen Mary University of London, London E1 4NS, United Kingdom*

^d*Dipartimento di Fisica ed Astronomia, Università di Catania and INFN, I-95123 Catania, Italy*

Abstract

What is the core of the human brain is a fundamental question that has been mainly addressed by studying the anatomical connections between differently specialized areas, thus neglecting the possible contributions from their functional interactions. While many methods are available to identify the core of a network when connections between nodes are all of the same type, a principled approach to define the core when multiple types of connectivity are allowed is still lacking. Here we introduce a general framework to define and extract the core-periphery structure of multi-layer networks by explicitly taking into account the connectivity patterns at each layer. We first validate our algorithm on synthetic networks of different size and density, and with tunable overlap between the cores at different layers. We then use our method to merge information from structural and functional brain networks, obtaining in this way an integrated description of the core of the human connectome. Results confirm the role of the main known cortical and subcortical hubs, but also suggest the presence of new areas in the sensori-motor cortex that are crucial for the intrinsic brain functioning. Taken together these findings provide fresh evidence on a fundamental question in modern neuroscience and offer new opportunities to explore the mesoscale properties of multimodal brain networks.

Keywords: Complex networks, Multilayer networks, Core-periphery structure, Rich-club, Brain connectivity, Multimodal integration

*Corresponding author

ICM, Hopital Pitie-Salpetriere
75013 Paris, France
Tel +33(0)157274294
Email fabrizio.devicofallani@gmail.com

1. Introduction

Complex networks are characterized by the existence of non-random structures at different topological scales [5–7]. A peculiar structure is the so-called core-periphery organization [8], where the network exhibits a group of tightly connected nodes (i.e. the *core*), and a group made by the remaining weakly connected nodes (i.e. the *periphery*).

Core-periphery organization has been recognized as a fundamental property of complex networks to support integration of information [9–16]. A related concept is that of rich-club behavior, where the tightly connected nodes are the network hubs, i.e. the nodes with a large number of links [17, 18]. A rich-club organization has been observed in various real-world systems, such as social, technological and biological networks [17–20], including the brain [21–24]. More recently, a refined version of the rich-club analysis, based not only on the number of connections of the hubs, but also on their capability to bridge different communities, has been shown to be relevant to support the integrative properties of the nervous system [25].

In the human brain, rich-club and rich-core organization, associated to the efficiency in communication and distribution of information, have been mainly reported in anatomical, or structural, connectivity networks obtained experimentally from diffusion tensor imaging (DTI) data. It has been conjectured that rich cores, rather than shortest paths, may actually be responsible for the efficient integration of information between remote brain areas [21], which is a crucial prerequisite for normal cognitive performance [26, 27]. Current evidence suggests that posterior medial and parietal cortical regions mainly constitute the core of the human connectome [21, 28], while they are contradictory on the role of other areas, such as the medial prefrontal cortex (mPFC) and the sensori-motor system, which are basic components of the brain functioning [49]. Because brain regions are also characterized by functional interactions inferred from neuroimaging data, such as functional magnetic resonance imaging (fMRI) [29, 30], we hypothesize that integrating information from both structural and functional networks can give a more accurate estimate of the regions that eventually constitute the core of the human cortex.

Instead of aggregating the two different types of connectivity or analyzing them separately, we adopt a multiplex network approach that preserves and exploits the original information on how brain regions are structurally and functionally interconnected. In a multiplex network, different connectivity types are mathematically represented as networks at different layers. Notably, in a multiplex - a particular case of multilayer network - there is a one-to-one correspondence between the nodes at different layers [31–35]. Multiplex network theory has been recently used to successfully extract higher-order properties of multimodal [36] and multifrequency brain networks that cannot be retrieved by standard approaches [37, 38].

Interestingly, the detection of core-periphery organization in multiplex networks has been poorly explored, with the exception of approaches based on k-core decomposition [42, 43]. To address this gap, we introduce a criterion to define and detect core-periphery organization in multiplex networks. Our method works for any number of layers and is scalable to large networks, being non-parametric and based on local node information [20]. In the following, we first introduce the general framework and then we validate it on synthetic multiplex networks with tunable core similarity.

We finally apply our method to integrate information from structural and functional brain networks and extract the multiplex core-periphery organization of the human brain.

47 The obtained results point to the main hubs known in the literature, but also allows to
 48 highlight the central role played by the regions of the sensori-motor system, which has
 49 been surprisingly neglected by previous studies on core-periphery organization, despite
 50 being considered a fundamental component of the default-mode network [49].
 51 Our research shades new light on the emergence of core regions in the human connectome,
 52 and we hope it will spur further work towards a better understanding of the complex
 53 relationships in the nervous system.

54 2. Results

55 2.1. *Extracting the rich core of a multiplex network*

56 Let us consider a multiplex network described by a vector of adjacency matrices $\mathcal{M} =$
 57 $\{A^{[1]}, \dots, A^{[M]}\}$, where all interactions of type α , $\alpha = 1, \dots, M$, are encoded in a different
 58 layer described by the adjacency matrix $A^{[\alpha]}$. To detect the core-periphery structure of
 59 a multiplex network, we first compute the multiplex degree vector $\mathbf{k}_i = \{k_i^{[1]}, \dots, k_i^{[M]}\}$
 60 of each node i [34]. From now on, we refer to $k_i^{[\alpha]}$, $\alpha = 1, \dots, M$, as the *richness* of node
 61 i at layer α . Notice that this is the simplest way to define the richness of a node, and
 62 different measures of richness, such as other measures of node centrality, can be as well
 63 used.

64 For each layer α , we then divide the links of node i in those towards lower richness
 65 nodes, and those towards higher richness nodes, so that we can decompose the degree of
 66 node i at layer α as $k_i^{[\alpha]} = k_i^{[\alpha]-} + k_i^{[\alpha]+}$. Finally, the *multiplex richness* μ_i of node i is
 67 obtained by aggregating single-layer information:

$$68 \quad \mu_i = \sum_{\alpha=1}^M c^{[\alpha]} k_i^{[\alpha]}. \quad (1)$$

69 where the coefficients $c^{[\alpha]}$ modulate the relative relevance of each layer and can, for
 70 instance, be determined by exogenous information. In analogy to the single-layer case,
 71 we define the multiplex richness of a node towards richer nodes as:

$$72 \quad \mu_i^+ = \sum_{\alpha=1}^M c^{[\alpha]} k_i^{[\alpha]+}. \quad (2)$$

73 In the most simple set-up we can assume $c^{[\alpha]} = c = 1/M \forall \alpha$. More general functional
 74 forms to aggregate the contributions from different layers, giving rise to alternative mea-
 75 sures of μ_i and μ_i^+ , are presented in the Methods section.

76 The nodes of the multiplex are ranked according to their richness μ , so that the node
 77 i with the best rank, i.e. $rank_i = 1$, is the node with the largest value of μ , the node
 78 ranked 2 is the one with the second largest value of μ , and so on. We then plot for each
 79 node i the value of μ_i^+ as a function of $rank_i$. The value of the rank corresponding to
 80 the maximum of μ_i^+ finally determines the core-periphery structure. All nodes with rank
 81 lower than such a value are assigned to the multiplex core, whereas the remaining ones
 82 become part of the periphery. We notice that also in the simplest case, when $c^{[\alpha]} = c \forall \alpha$,
 83 the multiplex core-periphery partition cannot be obtained by simply combining the cores

84 of the different layers, or by applying the single-layer algorithm on the corresponding
 85 aggregated network.

86 As an illustrative example, we report in Fig. 1 the curve μ_i^+ as a function of $rank_i$
 87 obtained in the case of the Top Noordin Terrorist network, a multiplex network of $N =$
 88 78 individuals with three layers (encoding information about mutual trust, common
 89 operations and exchanged communication between terrorists), which has been used as a
 90 benchmark to test measures and models of multiplex networks [34].

91 Coefficients $c^{[\alpha]}$ were chosen, in this case, to be inversely proportional to $K^{[\alpha]}$ to
 92 compensate for the different densities of the three layers. The resulting multiplex rich
 93 core integrates information from all the layers and looks different from the rich cores
 94 obtained at each of the three layers by a standard single-layer rich core analysis. More
 95 details about the results of this analysis are reported in Table S1.

96 2.2. Testing the method on multiplex networks with tunable core similarity

97 A network with a well defined core-periphery structure has a high density of links
 98 among core nodes. With a suitable labeling of the nodes, the adjacency matrix of the
 99 network can be decomposed into four different blocks: a dense diagonal block encoding
 100 information on core-core links, a sparser diagonal block describing links among peripheral
 101 nodes, and two off-diagonal blocks encoding core-periphery edges. The key feature of such
 102 block-structure is that $\rho_1 \gg \rho_3$, i.e. the density ρ_1 of the core-core block is much higher
 103 than that of the periphery-periphery block, ρ_3 . As first noted by Borgatti and Everett [8],
 104 the density ρ_2 of the off-diagonal blocks is typically not a crucial factor to characterize
 105 a core-periphery structure.

106 To test how our method works on multiplex networks with different structures, we
 107 have introduced a model to produce synthetic multiplex networks with tunable core
 108 similarity. In particular, we have constructed multiplexes where each of the $M = 2$
 109 layers contain $N = 250$ nodes and only $N_c = 50$ of them belong to the core. Each layer
 110 has the same average node degree $\langle k \rangle = 10$, and the same set of parameters $\rho_1 > \rho_2 > \rho_3$
 111 to describe its core-periphery structure. Our model allows to control the number of nodes
 112 that are both in the core of layer 1 and 2. (see Methods for more details).

113 To quantify the similarity among cores at different layers, we introduce the core
 114 similarity $S_c^{[\alpha]}$ of layer α with respect to the other layers as:

$$115 S_c^{[\alpha]} = \frac{1}{(M-1)} \sum_{\beta \neq \alpha}^M \frac{I_c^{[\alpha\beta]}}{N_c^{[\alpha]}}, \quad (3)$$

116 where $I_c^{[\alpha\beta]}$ is the number of nodes in the core of both layer α and layer β , whereas $N_c^{[\alpha]}$
 117 is the size of the core at layer α . The core similarity $S_c^{[\alpha]}$ ranges in $[0, 1]$. When layer α
 118 does not share core nodes with any other layers we have $S_c^{[\alpha]} = 0$, when all its core nodes
 119 also belong to the cores of the other layers $S_c^{[\alpha]} = 1$, and when on average only half of
 120 them are part of the cores on each other level $S_c^{[\alpha]} = 1/2$. The average core similarity of
 121 the multiplex can then be computed as $S_c = (1/M) \sum_{\alpha=1}^M S_c^{[\alpha]}$.

122 In Fig. 2 we show the results for three multiplex networks with different core similarity.
 123 In the left column of Fig. 2 we consider a multiplex with $S_c = 0$. The cores of the two
 124 layers are not overlapping, as shown in panel (a). As a consequence, many nodes with
 125 high degree in one layer have low degree in the other one. When $c^{[1]} = c^{[2]} = 0.5$, the

126 multiplex core of the system is formed by those nodes with sufficiently high multiplex
 127 richness, as shown in panel (b). In panel (c) we show the changes in the multiplex core
 128 when we partially ($c^{[1]} = 0.75, c^{[2]} = 0.25$, left subplot) or completely ($c^{[1]} = 1, c^{[2]} = 0$,
 129 right subplot) bias the algorithm towards the first layer.
 130 In the central column of Fig. 2 we consider a multiplex with $S_c = 1/2$. Half of the
 131 core nodes are in common to both layers while half are typical of each layer. The block
 132 structure of the two layers is partially overlapping, and the nodes are spread uniformly
 133 over the $k_i^{[2]}$ vs $k_i^{[1]}$ plane. In the unbiased case the multiplex core of the system is
 134 formed by nodes which are part of the core on both layers, but also by nodes scoring
 135 extremely high in one layer, despite being in the periphery in the other one (panel b).
 136 When $c^{[1]} > c^{[2]}$, this is particularly true for nodes which have high richness in the first
 137 layer and low richness in the second, while the opposite is much more unlikely (panel c).
 138 In the right column of Fig. 2 we consider a multiplex with $S_c \approx 1$. The block structure
 139 of the two layers is now almost identical; the node degrees $k^{[1]}$ and $k^{[2]}$ are correlated
 140 and most of the nodes belonging to each core are in the multiplex core (panel b). As
 141 the core structure at the two layers are extremely similar, the biased cases do not differ
 142 significantly from the unbiased one (panel c).

143 *2.3. Merging structure and function to extract the connectome's core*

144 We have applied our method to investigate the human connectome by considering, at
 145 the same time, structural and functional information. We have therefore constructed a
 146 multiplex brain network formed by one structural layer and one functional layer. The two
 147 layers were obtained by first averaging brain connectivity matrices estimated respectively
 148 from DTI and fMRI data in 171 healthy individuals. Each of the two layers is then
 149 thresholded by fixing the average node degree $\langle k \rangle$. We have focused our analysis on 158
 150 regions of interest (ROIs) of the cortex (see Methods for more details).

151 In Fig. 3 we report the cores found by analyzing separately the two layers, as well
 152 as the multiplex core obtained with our method. The figure refers to the case of a
 153 representative threshold corresponding to an average node degree $\langle k \rangle = 7$. We notice
 154 that the cores of the structural and functional layers are only partially overlapping, with
 155 a value of core similarity of $S_c = 0.15$. For the sake of completeness, we also report
 156 the S_c values for the the entire threshold range (Fig. S1). **A detailed analysis on the
 157 robustness of the multiplex core detection in presence of random fluctuations is reported
 158 in the Supplementary text S1.**

159 As shown in Fig. 3, ventral brain areas tend in general to form the structural core,
 160 while more dorsal regions appear in the functional core. Notably, brain regions of interest
 161 (ROIs, Table S2) that are in the core of both structural and functional layers also tend to
 162 be in the core of the multiplex. Instead, ROIs being in the periphery of both layers tend
 163 to be excluded from the multiplex core. However, exceptions may exist depending on the
 164 multiplex richness of the nodes. For example, the posterior part of the right precentral
 165 gyrus (RCGa3), which is in the periphery of both the structural and functional layer,
 166 is eventually assigned to the multiplex core, because of its relatively high rank score in
 167 the two layers. The situation appears even less predictable for ROIs that are in the
 168 core of one layer and in the periphery of the other layer. Only occasionally these will
 169 belong to the multiplex core. This is the case, for example, of the anterior part of right
 170 precentral gyrus (RCGa2) which exhibits a relatively low structural richness but high

171 functional richness, i.e. ranked seventh in the functional core, or of the anterior part of
172 the right parietal operculum (RPOC1), which has the highest structural richness but a
173 low functional richness.

174 **2.4. Revealing new core regions of the human brain**

175 We have extracted the multiplex core-periphery structure of the human brain for
176 the full range of available thresholds $\langle k \rangle = 1, 2, \dots, 120$ (see Methods for more details).
177 In this way, we have been able to calculate the *coreness* C_i of each node i , defined as
178 the normalized number of thresholds at which the corresponding ROI is present in the
179 rich core. This allows us to rank ROIs according to their likelihood to be part of the
180 multiplex core and to compare these to the rankings obtained separately for structural
181 and functional layers. We note that the same approach of investigating the persistence
182 across a set of different filtering thresholds can be applied to any node property. This
183 can turn useful for statistical validation in the case no threshold is universally accepted,
184 as often happens for brain networks [44–46].

185 Parietal (pre/cuneus PCU/LOC, superior parietal lobe SPL), cingulate (anterior Ca,
186 posterior Cp), temporal (superior temporal gyrus), insular (insular cortex IC), as well
187 as frontal ROIs (paracingulate PC) mainly constitute the structural core, as shown in
188 Fig. S2. While some overlap exists between the structural and the functional cores, the
189 latter rather tends instead to include occipital (occipital fusiform gyrus OFG, temporo-
190 occipital fusiform cortex TOFC) and central (pre/post central gyrus CGa/CGp) ROIs
191 and, notably, to exclude regions in the frontal lobe (top 25% ROIs, Fig. S3).

192 Fig. 4 shows the coreness of the multiplex network. As expected, ROIs that are
193 peripheral (i.e., low coreness) in both layers are also peripheral in the multiplex, while
194 ROIs with both a high structural and high functional coreness are typically observed in
195 the multiplex core (e.g., TOFC, OFG, Ca, Cp). Interesting behaviors emerge for those
196 regions typically characterized by high coreness in one layer and low coreness in the other
197 layer. In fact, some of these ROIs are part of the multiplex core, while others are usually
198 found in the multiplex periphery, as shown Fig. 5a. For areas with a different assignment
199 in the two layers, we note that the main contribution to the multiplex richness μ_i comes
200 from the richness in the layer where node i is identified as core. Interestingly, not only
201 the average richness of the node in the core layer is higher than the one in the peripheral
202 layer, but also its fluctuations around the mean.

203 As a consequence, among regions that are core in the structural layer but peripheral
204 in the functional one, those with relatively higher structural richness (degree), such as
205 precuneus PCU, insular cortex IC and posterior cingulate Cp, finally tend to join the
206 multiplex core no matter the exact value of their functional richness (upper right corner of
207 Fig. 5a). Conversely, ROIs with relatively lower structural degree are usually peripheral
208 in the multiplex, and typically located in the pre-frontal cortex PC and frontal lobe FP
209 (lower right corner of Fig. 5a), as illustrated in Fig. 5b,c. Similarly, among areas in the
210 functional core, those with relatively higher functional degree, such as precentral gyrus
211 CGa and central operculum COC, tend to join the multiplex core (upper left corner of
212 Fig. 5a). In contrast, ROIs with relatively lower functional degree, are mostly peripheral
213 in the multiplex, and are located in the parietal operculum POC and superior frontal
214 gyrus SFG (lower left corner of Fig. 5a).

215 **In a separate analysis, we have extracted the multiplex brain coreness from each**
216 **individual and we show that, despite a normal inter-subject variability, the average mul-**

217 tiplex brain coreness is very similar to the multiplex coreness of the group-averaged brain
218 networks (Fig. S4). Finally, we have evaluated the robustness of the results when also in-
219 cluding subcortical ROIs in the brain networks. We report that thalamus, putamen and
220 hippocampus are among the regions with highest coreness and therefore become part of
221 the multiplex core (Fig. S5). Interestingly, their presence does not significantly alter the
222 coreness of the other ROIs (Fig. S6), suggesting an assortative structure where highly
223 connected subcortical regions preferentially get connected with regions in the cortex.

224 3. Discussion

225 The existence of a network core in the brain is a prerequisite for neural functioning
226 and cognition, and damages to the core have been associated with several neurological
227 or psychiatric diseases [23, 47, 48]. Finding the router regions that ensure integration
228 between the different brain modules and communication in the system is therefore a
229 fundamental question in neuroscience. Previous studies have addressed the question by
230 considering only the structural connectivity of the brain through disparate techniques,
231 such as k -core decomposition, centrality measures, and rich-club analysis [21, 28]. While
232 the obtained results agree on the implication of posterior medial and parietal cortical
233 regions - as well as subcortical thalamus, putamen and hippocampus - in the network
234 core [21, 28], they neglect the possible role of other areas which are crucial from a
235 functional perspective, such as those in the default-mode network (DMN) [49].

236 To integrate information from both structural and functional brain connectivity at
237 the network level, we introduce a general criterion to define and extract the core when
238 nodes are connected through links which can vary in meaning and nature, and the whole
239 system can be described as a network with multiple layers [31–35]. Compared to standard
240 approaches, this method has the theoretical advantage to provide a more robust solution,
241 taking into account the relative importance of the nodes at each layer, rather than simply
242 considering the union or intersection of the cores across layers, or extracting the core from
243 the aggregated network.

244 The obtained results shed new light on the role of the regions characterizing the
245 intrinsic brain function to eventually shape the core of the human brain. First, we show
246 that mPFC (e.g., PC and FP), exhibiting a high structural but low functional coreness,
247 is eventually assigned to the periphery (Fig. 5a, lower-right corner). This outcome can
248 be predicted by the lower multiplex richness and relatively low structural degree, and not
249 by the solely attitude of frontal areas to be peripheral in the functional brain network
250 (Fig. 5b,c). The exclusion of the mPFC from the rich core supports the hypothesis that
251 default-mode network activity may be mainly driven from highly coupled areas of the
252 posterior medial and parietal cortex, which in turn link to other highly connected regions,
253 such as the medial orbitofrontal cortex [28].

254 Second, while frontal ROIs are excluded, new regions gain importance and become
255 part of the core because of their higher multiplex richness (see Fig. 5a, upper left
256 corner). Among them, we report areas of the central gyrus (CGa, CGp to a minor
257 extent), which are characterized by a low structural but relatively high functional degree,
258 as shown in Fig. 5b,c. These regions are part of the primary sensori-motor cortex, which
259 has been shown to be the most extensive of the resting-state components, or networks
260 (out of 8 [50]), covering 27% percent of the total gray matter in the brain [51]. The
261 primary sensori-motor component has a high degree of integration (overlap and activity

262 coupling) with all other resting-state networks (e.g., DMN), which is consistent with the
263 increased synchronization of neural activity in cortical regions during sensory processing
264 [52]. Notably, ongoing functional connectivity in the primary sensori-motor network,
265 originally revealed by seed-based analysis [53, 54], has been extensively verified by ICA
266 and clustering methods [55, 56].

267 Our method provides an effective tool to integrate mesoscale topological informa-
268 tion in brain networks derived from multimodal neuroimaging data. Multimodal inte-
269 gration of brain networks is gaining more and more interest [57–60] due, on the one
270 hand, to the increasing availability of large heterogenous datasets (e.g. HCP <http://www.humanconnectomeproject.org>, ADNI <http://adni.loni.usc.edu>) and, on the
271 other hand, to the need of principled ways to characterize multiscale neural mechanisms
272 (e.g., cross-frequency coupling) and provide predictive diagnostics for multifactor brain
273 diseases, such as Alzheimer’s disease.
274

275 It is important to note, that our analysis of the human connectome relies on the
276 assumption that each layer contributes with the same intensity to the definition of the
277 multiplex core. In general, however, the contribution of a layer α can be weighted
278 differently through an opportune choice of the parameter $c^{[\alpha]}$, and this can be used to
279 enhance or reduce the importance of the different types of connectivity. A larger value
280 of $c^{[\alpha]}$ increases the relevance of the corresponding layer until when, in the limit in which
281 $c^{[\alpha]} \rightarrow 1$ and the coefficients of all the other layers go to zero, the multiplex core is not
282 any more defined by the topology of all the M layers, but coincides with the core at layer
283 α . For instance, setting $c^{[structural]} = 1$ and $c^{[functional]} = 0$ returns a core based on
284 the anatomical information only, and in agreement with most of the previous literature
285 on such topic (see Fig. S2). As an unbiased way to characterize the multiplex core of
286 the human brain, we have focused our analysis on the simplest and symmetric case,
287 $c^{[structural]} = c^{[functional]} = 0.5$. **We show in Fig. S7 that the results are relatively stable**
288 **for small perturbations around this unbiased condition.** However, other combinations
289 are in general possible and should be adopted if supported by a plausible rationale. For
290 example, in the case of multifrequency brain networks, one could assign stronger weights
291 to higher frequency layers in order to compensate for $1/f$ frequency scaling of power
292 spectra [61].

293 From an operative point of view, the proposed method to detect the core-periphery
294 organization in multiplex networks has two clear advantages: *i*) it is fast and scalable,
295 since it works using only local information; *ii*) it is non-parametric, e.g. no need to
296 input *a-priori* information such as the core size. Moreover, it can be generalized in
297 a straightforward way to the case of directed networks. A drawback of the method
298 is that it focuses on highly connected rich nodes, and neglects the possible important
299 role of the so-called *connectors*, i.e. central nodes with low degree [62]. We note that
300 alternative core-periphery structures which include connectors can be detected by more
301 computationally demanding methods such as those based on stochastic block models,
302 which have been recently proposed to extract the mesoscale structure of time-varying
303 and multilayer networks [63]. We hope that our work can trigger further developments
304 in the exploration of core-periphery structure of real-world large-scale multiplex networks.

305 To conclude, our method to investigate multiplex core-periphery organization in com-
306 plex networks suggests that the core of the human cortex is made up of known cortical
307 and subcortical hubs, as well as of areas in the sensori-motor system that were previously
308 overlooked by standard approaches, but that are crucial for the brain functioning. Our

309 findings offer an augmented definition of the rich core of the human brain, which takes
310 into account not only the anatomical structure but also its function.

311 **We hope that our work will contribute to advance our understanding of the mesoscale**
312 **connectivity mechanisms in multiplex brain networks, in an effort to better integrate the**
313 **one-to-many relationships that exist between structure and function in the human brain**
314 **[29].**

315 4. Methods

316 4.1. *Multiplex stochastic block model with tunable core similarity*

317 Stochastic block models for multiplex networks have been recently introduced by
318 Peixoto [63]. Here, we introduce a stochastic block model that allows to sample multiplex
319 networks with an assigned value of core similarity S_C (see Eq. 3). Suppose we have N
320 nodes and we want to construct a multiplex network having a core-periphery structure
321 at each layer $\alpha = 1, \dots, M$, with $N_c^{[\alpha]}$ nodes in the core of layer α .

322 In particular, we set $M = 2$, $N = 250$, $N_c^{[1]} = N_c^{[2]} = N_c = 50$, and we create at each
323 layer a core-periphery structure with the same set of densities: $\rho_1 = 0.2$, $\rho_2 = 0.04$ and
324 $\rho_3 = 0.03$. Namely, for each of the two layers, we connect with a probability ρ_1 two nodes
325 both in the core, with probability ρ_2 a node in the core and a node in the periphery,
326 and finally with probability ρ_3 two peripheral nodes. The values of the three parameters
327 were chosen in a way that $\langle k \rangle = 10$ on both layers, and the core-periphery structure of
328 each layer is sufficiently strong to be detected with good accuracy, as discussed in the
329 Supplementary text S2.

330 Different levels of core similarity are achieved by varying the overlap between core
331 nodes at the two layers. When the two sets of core nodes are completely overlapping,
332 $S_c = 1$, whereas when the two sets are disjoint $S_c = 0$. Despite other related formulations
333 of S_c are possible, our definition reflects the intuition that when two layers with equal
334 core size share half of the core nodes, then $S_c = 1/2$.

335 4.2. *Multiplex richness μ_i and μ_i^+*

336 The multiplex richness μ_i and μ_i^+ introduced in Eqs. 1 and 2 are obtained by mean
337 of a simple aggregation of information based on the single layers. In the simplest set-up
338 $c^{[\alpha]} = c = 1/M$ for $\alpha = 1, \dots, M$, and the multiplex richness μ_i of a node i is simply
339 proportional to its overlapping degree o_i [34]. A layer with higher density weighs more
340 in the computation of the multiplex core of a network.

341 In general, coefficients $c^{[\alpha]}$ can be used to modulate the relevance to the layers of the
342 network in order to extract its core. If one wants to have equal contributions to μ_i and
343 μ_i^+ from all the layers but their number of links $K^{[\alpha]}$ is different - for instance because
344 in some layers it might be easier to establish or measure a connection than in others - a
345 natural choice is to set $c^{[\alpha]}$ to be proportional to $1/K^{[\alpha]}$. In other cases, independently
346 from their density, it might be reasonable to assign different importance to different
347 layers, because of exogenous information. Once again this can be achieved by assigning
348 different values of the coefficients $c^{[\alpha]}$.

349 At last, we notice that Eq. 1 is a particular choice of a more general scenario, where
 350 the multiplex richness μ_i is a generic function f of the degree of a node at the different
 351 layers:

$$352 \quad \mu_i = f(k_i^{[1]}, \dots, k_i^{[M]}). \quad (4)$$

353 and μ_i^+ is a function of a generic function g :

$$354 \quad \mu_i^+ = g(k_i^{+[1]}, \dots, k_i^{+[M]}). \quad (5)$$

355 4.3. Multimodal brain networks

356 We have considered 171 healthy human subjects from the NKI Rockland dataset
 357 http://fcon_1000.projects.nitrc.org/indi/pro/nki.html. We have used diffusion
 358 weighted magnetic resonance imaging (dwMRI) and functional magnetic resonance imag-
 359 ing (fMRI) to derive respectively structural and functional brain networks in each subject.

360 We have gathered the corresponding connectivity matrices from the USC Multimodal
 361 Connectivity Database (<http://umcd.humanconnectomeproject.org>) [64].

362 In particular, structural connectivity have been obtained using anatomical fiber as-
 363 signment through the continuous tracking (FACT) algorithm [65]. Functional connectiv-
 364 ity has been computed by means of the Pearson’s correlation coefficient between fMRI
 365 signals recorded during a 10 minute resting state (RS). RS-based functional connectivity
 366 measures the amount of interaction - or temporal dependence - between different brain
 367 areas during spontaneous brain activity [30]. More details about the processing steps can
 368 be found here [66]. A total number of $N = 188$ regions of interest (ROIs) are available
 369 for both structural and functional brain networks, thus resulting in connectivity matrices
 370 of size $N \times N$, spatially matched with the MNI152 template [67].

371 Because we are mainly interested in cortical networks, we focused our analysis on the
 372 network obtained by removing all subcortical ROIs and obtained connectivity matrices
 373 of size 158×158 . The results for all the ROIs are reported for the sake of completeness.
 374 The full name and acronym for all the ROIs can be found in Table S1. We have then
 375 averaged the resulting connectivity matrices (after Fisher transformation) across subjects
 376 in order to have a population-level representation. At the end, we have obtained a struc-
 377 tural weighted connectivity matrix \mathcal{S} , whose entry $s_{ij} = s_{ji}$ contained the group-average
 378 number of axonal fibers between ROIs i and j , and a functional weighted connectivity
 379 matrix \mathcal{F} , whose entry $f_{ij} = f_{ji}$ corresponded to the group-average correlation coefficient
 380 between the fMRI signals of ROIs i and j .

381 We have used density-based thresholding to derive structural and functional brain
 382 networks by removing the lowest values from the connectivity matrices and binarizing the
 383 remaining ones [30]. We have considered a full range of density thresholds, corresponding
 384 to an increasing average node degree $\langle k \rangle = 1, 2, \dots, 120$. The last value was given by the
 385 maximal $\langle k \rangle$ observed in the native structural connectivity matrices, which are originally
 386 not fully connected. After filtering, for each threshold we have combined the resulting
 387 structural and functional brain networks into a multiplex network $\mathcal{M} = \{\mathcal{S}, \mathcal{F}\}$.

388 Competing interests

389 We have no competing interests.

390 Authors' contributions

391 FB carried out the theoretical work, participated in data analysis, participated in
392 the design of the study and drafted the manuscript; JG participated in data analysis
393 and drafted the manuscript; MC conceived and designed the study, and helped draft the
394 manuscript. VL conceived the study and drafted the manuscript; FDVF coordinated the
395 study, participated in the design of the study, participated in data analysis and drafted
396 the manuscript. All authors gave final approval for publication.

397 Funder

398 FDVF and MC acknowledge support by the ANR French program through the con-
399 tracts ANR-10-IAIHU-06 and ANR-15-NEUC-0006-02. The funders had no role in study
400 design, data collection and analysis, decision to publish, or preparation of the manuscript.

401 References

- 402 [1] R. Albert, A.-L. Barabasi, Statistical mechanics of complex networks, *Reviews of Modern Physics*
403 74 (1) (2002) 47–97. doi:10.1103/RevModPhys.74.47.
- 404 [2] M. Newman, The Structure and Function of Complex Networks, *SIAM Review* 45 (2) (2003) 167–
405 256. doi:10.1137/S003614450342480.
- 406 [3] S. Boccaletti, V. Latora, Y. Moreno, M. Chavez, D. U. Hwang, Complex networks: Structure and
407 dynamics, *Physics Reports* 424 (4) (2006) 175–308. doi:10.1016/j.physrep.2005.10.009.
- 408 [4] V. Latora, V. Nicosia, G. Russo, *Complex Networks: Principles, Methods and Applications*, Cam-
409 bridge University Press, 2017, google-Books-ID: qV0yDwAAQBAJ.
- 410 [5] R. Milo, S. Shen-Orr, S. Itzkovitz, N. Kashtan, D. Chklovskii, U. Alon, Network Mo-
411 tifs: Simple Building Blocks of Complex Networks, *Science* 298 (5594) (2002) 824–827.
412 doi:10.1126/science.298.5594.824.
- 413 [6] M. Girvan, M. E. J. Newman, Community structure in social and biological networks, *Proceedings*
414 *of the National Academy of Sciences* 99 (12) (2002) 7821–7826. doi:10.1073/pnas.122653799.
- 415 [7] S. Fortunato, Community detection in graphs, *Physics Reports* 486 (35) (2010) 75–174.
416 doi:10.1016/j.physrep.2009.11.002.
- 417 [8] S. P. Borgatti, M. G. Everett, Models of core/periphery structures, *Social Networks* 21 (4) (2000)
418 375–395. doi:10.1016/S0378-8733(99)00019-2.
- 419 [9] P. Csermely, A. London, L.-Y. Wu, B. Uzzi, Structure and dynamics of core/periphery networks,
420 *Journal of Complex Networks* 1 (2) (2013) 93–123. doi:10.1093/comnet/cnt016.
- 421 [10] M. Rombach, M. Porter, J. Fowler, P. Mucha, Core-Periphery Structure in Networks, *SIAM Journal*
422 *on Applied Mathematics* 74 (1) (2014) 167–190. doi:10.1137/120881683.
- 423 [11] X. Zhang, T. Martin, M. E. J. Newman, Identification of core-periphery structure in networks,
424 *Physical Review E* 91 (3) (2015) 032803. doi:10.1103/PhysRevE.91.032803.
- 425 [12] P. Barucca, F. Lillo, Disentangling bipartite and core-periphery structure in financial networks,
426 *Chaos, Solitons & Fractals* 88. doi:10.1016/j.chaos.2016.02.004.
- 427 [13] T. Verma, F. Russmann, N. a. M. Arajo, J. Nagler, H. J. Herrmann, Emergence of coreperipheries
428 in networks, *Nature Communications* 7 (2016) 10441. doi:10.1038/ncomms10441.
- 429 [14] G. Fagiolo, J. Reyes, S. Schiavo, The evolution of the world trade web: a weighted-network analysis,
430 *Journal of Evolutionary Economics* 20 (4) (2010) 479–514. doi:10.1007/s00191-009-0160-x.
- 431 [15] J. P. Boyd, W. J. Fitzgerald, M. C. Mahutga, D. A. Smith, Computing continuous core/periphery
432 structures for social relations data with MINRES/SVD, *Social Networks* 32 (2) (2010) 125–137.
433 doi:10.1016/j.socnet.2009.09.003.
- 434 [16] F. Luo, B. Li, X.-F. Wan, R. H. Scheuermann, Core and periphery structures in protein interaction
435 networks, *BMC Bioinformatics* 10 (4) (2009) S8. doi:10.1186/1471-2105-10-S4-S8.
- 436 [17] V. Colizza, A. Flammini, M. A. Serrano, A. Vespignani, Detecting rich-club ordering in complex
437 networks, *Nature Physics* 2 (2) (2006) 110. doi:10.1038/nphys209.
- 438 [18] S. Zhou, R. J. Mondragon, The rich-club phenomenon in the Internet topology, *IEEE Communica-*
439 *tions Letters* 8 (3) (2004) 180–182. doi:10.1109/LCOMM.2004.823426.

- 440 [19] L. M. Vaquero, M. Cebrian, The rich club phenomenon in the classroom, *Scientific Reports* 3 (2013)
441 1174. doi:10.1038/srep01174.
- 442 [20] A. Ma, R. J. Mondragón, Rich-Cores in Networks, *PLOS ONE* 10 (3) (2015) e0119678.
443 doi:10.1371/journal.pone.0119678.
- 444 [21] M. P. v. d. Heuvel, O. Sporns, Rich-Club Organization of the Human Connectome, *The Journal of*
445 *Neuroscience* 31 (44) (2011) 15775–15786. doi:10.1523/JNEUROSCI.3539-11.2011.
- 446 [22] L. Harriger, M. P. v. d. Heuvel, O. Sporns, Rich Club Organization of Macaque Cere-
447 *bral Cortex and Its Role in Network Communication*, *PLOS ONE* 7 (9) (2012) e46497.
448 doi:10.1371/journal.pone.0046497.
- 449 [23] M. P. van den Heuvel, O. Sporns, G. Collin, T. Scheewe, R. C. W. Mandl, W. Cahn, J. Goi,
450 H. E. Hulshoff Pol, R. S. Kahn, Abnormal rich club organization and functional brain dynamics in
451 schizophrenia, *JAMA psychiatry* 70 (8) (2013) 783–792. doi:10.1001/jamapsychiatry.2013.1328.
- 452 [24] G. Ball, P. Aljabar, S. Zebari, N. Tusor, T. Arichi, N. Merchant, E. C. Robinson, E. Ogun-
453 *dipe*, D. Rueckert, A. D. Edwards, S. J. Counsell, Rich-club organization of the newborn hu-
454 *man brain*, *Proceedings of the National Academy of Sciences* 111 (20) (2014) 7456–7461.
455 doi:10.1073/pnas.1324118111.
- 456 [25] M. A. Bertolero, B. T. T. Yeo, M. DEsposito, The diverse club, *Nature Communications* 8 (1)
457 (2017) 1277. doi:10.1038/s41467-017-01189-w.
- 458 [26] E. Bullmore, O. Sporns, Complex brain networks: graph theoretical analysis of structural and
459 *functional systems*, *Nature Reviews Neuroscience* 10 (3) (2009) 186–198. doi:10.1038/nrn2575.
- 460 [27] C. J. Stam, Modern network science of neurological disorders, *Nature Reviews. Neuroscience* 15 (10)
461 (2014) 683–695. doi:10.1038/nrn3801.
- 462 [28] P. Hagmann, L. Cammoun, X. Gigandet, R. Meuli, C. J. Honey, V. J. Wedeen,
463 *O. Sporns*, Mapping the Structural Core of Human Cerebral Cortex, *PLoS Biology* 6 (7).
464 doi:10.1371/journal.pbio.0060159.
- 465 [29] K. J. Friston, Functional and effective connectivity: a review, *Brain connectivity* 1 (1) (2011) 13–36.
466 doi:10.1089/brain.2011.0008.
- 467 [30] F. De Vico Fallani, J. Richiardi, M. Chavez, S. Achard, Graph analysis of functional brain networks:
468 *practical issues in translational neuroscience*, *Philosophical Transactions of the Royal Society B:*
469 *Biological Sciences* 369 (1653) (2014) 20130521. doi:10.1098/rstb.2013.0521.
- 470 [31] M. De Domenico, A. Sol-Ribalta, E. Cozzo, M. Kivel, Y. Moreno, M. A. Porter, S. Gmez, A. Aren-
471 *nas*, Mathematical Formulation of Multilayer Networks, *Physical Review X* 3 (4) (2013) 041022.
472 doi:10.1103/PhysRevX.3.041022.
- 473 [32] M. Kivel, A. Arenas, M. Barthelemy, J. P. Gleeson, Y. Moreno, M. A. Porter, Multilayer networks,
474 *Journal of Complex Networks* (2014) cnu016doi:10.1093/comnet/cnu016.
- 475 [33] S. Boccaletti, G. Bianconi, R. Criado, C. I. del Genio, J. Gmez-Gardees, M. Romance, I. Sendia-
476 *Nadal*, Z. Wang, M. Zanin, The structure and dynamics of multilayer networks, *Physics Reports*
477 544 (1) (2014) 1–122. doi:10.1016/j.physrep.2014.07.001.
- 478 [34] F. Battiston, V. Nicosia, V. Latora, Structural measures for multiplex networks, *Physical Review*
479 *E* 89 (3) (2014) 032804. doi:10.1103/PhysRevE.89.032804.
- 480 [35] F. Battiston, V. Nicosia, V. Latora, The new challenges of multiplex networks: Measures and mod-
481 *els*, *The European Physical Journal Special Topics* 226 (3) (2017) 401–416. doi:10.1140/epjst/e2016-
482 60274-8.
- 483 [36] F. Battiston, V. Nicosia, M. Chavez, V. Latora, Multilayer motif analysis of brain networks, *Chaos:*
484 *An Interdisciplinary Journal of Nonlinear Science* 27 (4) (2017) 047404. doi:10.1063/1.4979282.
- 485 [37] M. De Domenico, S. Sasai, A. Arenas, Mapping Multiplex Hubs in Human Functional Brain Net-
486 *works*, *Frontiers in Neuroscience* 10 (2016) 326. doi:10.3389/fnins.2016.00326.
- 487 [38] J. Guillon, Y. Attal, O. Colliot, V. L. Corte, B. Dubois, D. Schwartz, M. Chavez, F. De Vico Fallani,
488 *Loss of brain inter-frequency hubs in Alzheimer’s disease*, *Scientific Reports* 7 (1) (2017) 10879.
489 doi:10.1038/s41598-017-07846-w.
- 490 [39] P. J. Mucha, T. Richardson, K. Macon, M. A. Porter, J.-P. Onnela, Community Structure
491 *in Time-Dependent, Multiscale, and Multiplex Networks*, *Science* 328 (5980) (2010) 876–878.
492 doi:10.1126/science.1184819.
- 493 [40] M. De Domenico, A. Lancichinetti, A. Arenas, M. Rosvall, Identifying Modular Flows on Multilayer
494 *Networks Reveals Highly Overlapping Organization in Interconnected Systems*, *Physical Review X*
495 5 (1) (2015) 011027. doi:10.1103/PhysRevX.5.011027.
- 496 [41] F. Battiston, J. Iacovacci, V. Nicosia, G. Bianconi, V. Latora, Emergence of Multiplex Communities
497 *in Collaboration Networks*, *PLOS ONE* 11 (1) (2016) e0147451. doi:10.1371/journal.pone.0147451.
- 498 [42] N. Azimi-Tafreshi, J. Gmez-Gardees, S. N. Dorogovtsev, k-core percolation on multiplex net-

- works, *Physical Review E, Statistical, Nonlinear, and Soft Matter Physics* 90 (3) (2014) 032816. doi:10.1103/PhysRevE.90.032816.
- [43] B. Corominas-Murtra, S. Thurner, The Weak Core and the Structure of Elites in Social Multiplex Networks, in: *Interconnected Networks, Understanding Complex Systems*, Springer, Cham, 2016, pp. 165–177, doi: 10.1007/978-3-319-23947-7_10.
- [44] B. C. M. van Wijk, C. J. Stam, A. Daffertshofer, Comparing Brain Networks of Different Size and Connectivity Density Using Graph Theory, *PLoS ONE* 5 (10) (2010) e13701. doi:10.1371/journal.pone.0013701.
- [45] A. Fornito, A. Zalesky, M. Breakspear, Graph analysis of the human connectome: Promise, progress, and pitfalls, *NeuroImage* 80 (2013) 426–444. doi:10.1016/j.neuroimage.2013.04.087.
- [46] F. De Vico Fallani, V. Latora, M. Chavez, A Topological Criterion for Filtering Information in Complex Brain Networks, *PLOS Computational Biology* 13 (1) (2017) e1005305. doi:10.1371/journal.pcbi.1005305.
- [47] L. L. Gollo, A. Zalesky, R. M. Hutchison, M. van den Heuvel, M. Breakspear, Dwelling quietly in the rich club: brain network determinants of slow cortical fluctuations, *Philosophical Transactions of the Royal Society B: Biological Sciences* 370 (1668). doi:10.1098/rstb.2014.0165.
- [48] M. Daianu, N. Jahanshad, T. M. Nir, C. R. Jack, M. W. Weiner, M. A. Bernstein, P. M. Thompson, Alzheimer’s Disease Neuroimaging Initiative, Rich club analysis in the Alzheimer’s disease connectome reveals a relatively undisturbed structural core network, *Human Brain Mapping* 36 (8) (2015) 3087–3103. doi:10.1002/hbm.22830.
- [49] R. L. Buckner, J. R. Andrews-Hanna, D. L. Schacter, The Brain’s Default Network, *Annals of the New York Academy of Sciences* 1124 (1) (2008) 1–38. doi:10.1196/annals.1440.011.
- [50] M. P. v. d. Heuvel, H. E. H. Pol, Exploring the brain network: A review on resting-state fMRI functional connectivity, *European Neuropsychopharmacology* 20 (8) (2010) 519–534. doi:10.1016/j.euroneuro.2010.03.008.
- [51] D. Tomasi, N. D. Volkow, Association between Functional Connectivity Hubs and Brain Networks, *Cerebral Cortex* 21 (9) (2011) 2003–2013. doi:10.1093/cercor/bhq268.
- [52] R. Srinivasan, D. P. Russell, G. M. Edelman, G. Tononi, Increased Synchronization of Neuromagnetic Responses during Conscious Perception, *Journal of Neuroscience* 19 (13) (1999) 5435–5448.
- [53] B. Biswal, F. Zerrin Yetkin, V. M. Haughton, J. S. Hyde, Functional connectivity in the motor cortex of resting human brain using echo-planar mri, *Magnetic Resonance in Medicine* 34 (4) (1995) 537–541. doi:10.1002/mrm.1910340409.
- [54] J. Xiong, L. M. Parsons, J. H. Gao, P. T. Fox, Interregional connectivity to primary motor cortex revealed using MRI resting state images, *Human Brain Mapping* 8 (2-3) (1999) 151–156.
- [55] R. Salvador, J. Suckling, M. Coleman, J. Pickard, D. Menon, E. Bullmore, Neurophysiological architecture of functional magnetic resonance images of human brain, *Cerebral Cortex* 15 (9) (2005) 1332–2342.
- [56] J. Damoiseaux, S. Rombouts, F. Barkhof, P. Scheltens, C. Stam, S. Smith, C. Beckmann, Consistent resting-state networks across healthy subjects, *Proceedings of the National Academy of Sciences of the United States of America* 103 (37) (2006) 13848–13853.
- [57] E. Rykhlevskaia, G. Gratton, M. Fabiani, Combining structural and functional neuroimaging data for studying brain connectivity: A review, *Psychophysiology* 45 (2) (2008) 173–187. doi:10.1111/j.1469-8986.2007.00621.x.
- [58] X. Lei, D. Ostwald, J. Hu, C. Qiu, C. Porcaro, A. P. Bagshaw, D. Yao, Multimodal Functional Network Connectivity: An EEG-fMRI Fusion in Network Space, *PLOS ONE* 6 (9) (2011) e24642. doi:10.1371/journal.pone.0024642.
- [59] T. Simas, M. Chavez, P. R. Rodriguez, A. Diaz-Guilera, An algebraic topological method for multimodal brain networks comparisons, *Frontiers in Psychology* 6 (2015) 904. doi:10.3389/fpsyg.2015.00904.
- [60] E. Amico, J. Goi, Mapping hybrid functional-structural connectivity traits in the human connectome, arXiv:1710.02199 [q-bio]ArXiv: 1710.02199.
- [61] C. Bzdard, H. Krger, A. Destexhe, Does the $1/f$ Frequency Scaling of Brain Signals Reflect Self-Organized Critical States?, *Physical Review Letters* 97 (11) (2006) 118102. doi:10.1103/PhysRevLett.97.118102.
- [62] B. Corominas-Murtra, B. Fuchs, S. Thurner, Detection of the Elite Structure in a Virtual Multiplex Social System by Means of a Generalised K-Core, *PLOS ONE* 9 (12) (2014) e112606. doi:10.1371/journal.pone.0112606.
- [63] T. P. Peixoto, Inferring the mesoscale structure of layered, edge-valued, and time-varying networks, *Physical Review E* 92 (4) (2015) 042807. doi:10.1103/PhysRevE.92.042807.

- 558 [64] J. A. Brown, J. D. Van Horn, Connected brains and mindsThe UMCD repository for brain connec-
559 tivity matrices, *NeuroImage* 124 (Part B) (2016) 1238–1241. doi:10.1016/j.neuroimage.2015.08.043.
- 560 [65] S. Mori, P. C. M. van Zijl, Fiber tracking: principles and strategies a technical review, *NMR in*
561 *Biomedicine* 15 (7-8) (2002) 468–480. doi:10.1002/nbm.781.
- 562 [66] J. A. Brown, J. D. Rudie, A. Bandrowski, V. Horn, J. D, S. Y. Bookheimer, The UCLA multimodal
563 connectivity database: a web-based platform for brain connectivity matrix sharing and analysis,
564 *Frontiers in Neuroinformatics* 6. doi:10.3389/fninf.2012.00028.
- 565 [67] R. C. Craddock, G. James, P. E. Holtzheimer, X. P. Hu, H. S. Mayberg, A whole brain fMRI
566 atlas generated via spatially constrained spectral clustering, *Human Brain Mapping* 33 (8) (2012)
567 1914–1928. doi:10.1002/hbm.21333.

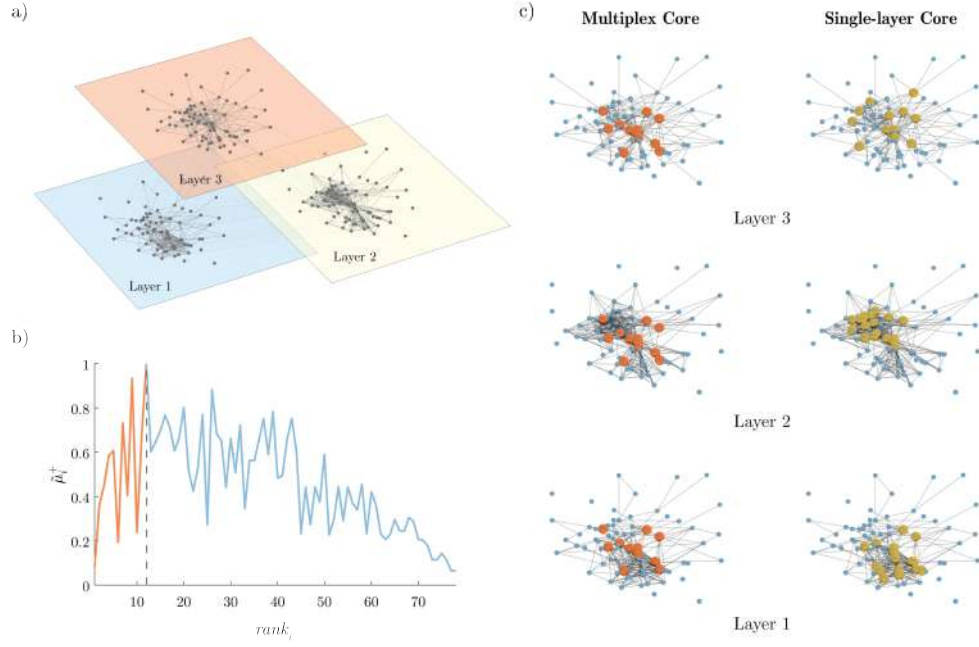


Figure 1: **An illustrative example of the multiplex rich core analysis.** In panel (a) we show a multiplex social network obtained from the Top Noordin Terrorists' contacts, with $N = 78$ nodes, $M = 3$ layers and $K^{[1]} = 259$, $K^{[2]} = 437$ and $K^{[3]} = 200$, for the three layers respectively. Panel b) shows the curve $\tilde{\mu}_i^+ = \mu_i^+ / \max(\mu_i^+)$ as a function of $rank_i$. All nodes from rank equal to 1 up to the node with maximum $\tilde{\mu}^+$ are part of the core of the multiplex, which is shown in red color in panel (c), first column. The cores obtained at each layer by the standard single-layer analysis are reported in yellow for the sake of comparison in the second column. The percentages of core nodes in the single layers that are in the multiplex core are respectively 83.3% for layer 1, 66.7% for layer 2, and 58.3% for layer 3

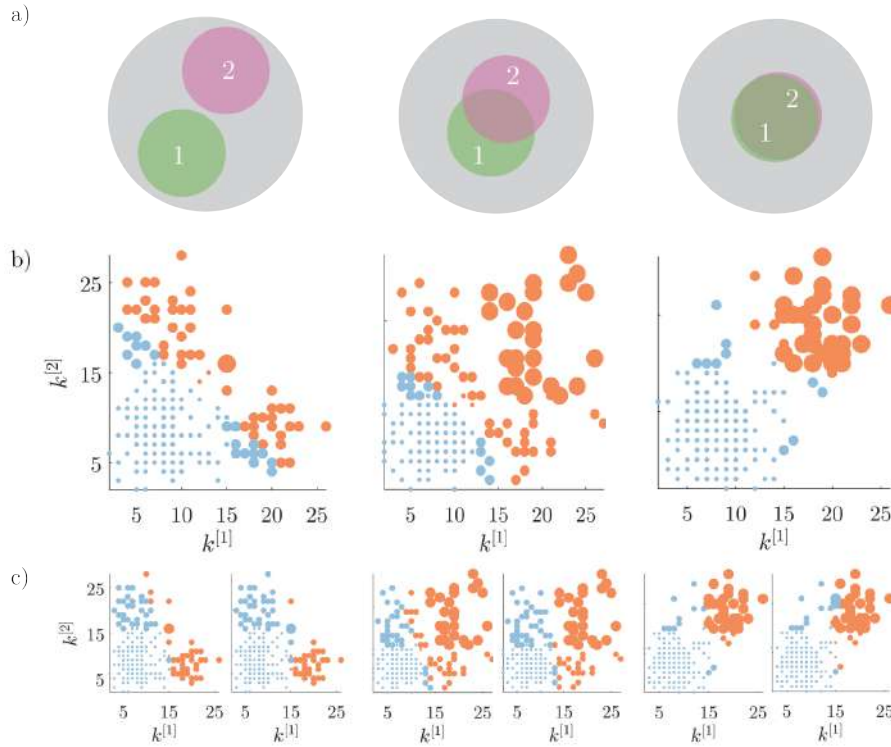


Figure 2: **Core-periphery structure in synthetic multiplex networks with different core similarity.** In panel (a) we sketch multiplex networks with $M = 2$ layers, $N = 250$ nodes and different levels of core similarity, namely $S_c = 0$ (left column), $S_c = 1/2$ (central column) and $S_c = 1$ (right column). In panel (b) the nodes are placed in a two dimensional plane according to their degree at each layer. The size of each dot is proportional to the multiplex richness μ_i of the node (with $c^{[1]} = 1, c^{[2]} = 0$). Nodes belonging to the multiplex cores are usually placed in the right-top corner of the plots and are colored orange, while the multiplex periphery is in blue. In panel (c) we report results obtained for two cases with $c^{[1]} \neq c^{[2]}$, namely: $(c^{[1]} = 0.75, c^{[2]} = 0.25)$ where the core is biased towards the important nodes of the first layer (left), and $(c^{[1]} = 1, c^{[2]} = 0)$, where the core corresponds to the core of the first layer (right).

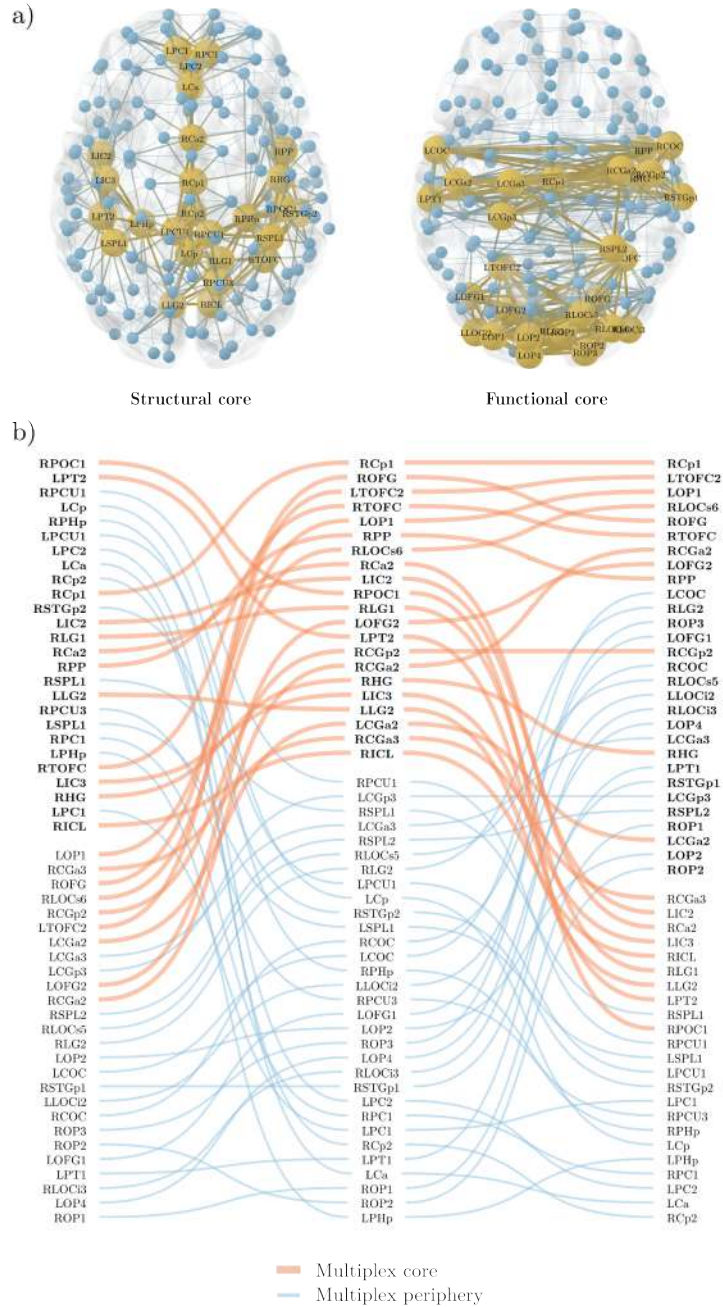


Figure 3: **Extracting the multiplex core of the human brain from structural and functional information.** Panel a) The structural and functional brain networks filtered with an average node degree $\langle k \rangle = 7$ are shown respectively on the left and right side. They are represented from above with the frontal lobe pointing upward. The position of the nodes corresponds to the actual location of the brain regions of interests (ROIs, Table S2). Yellow and large nodes represent the brain regions belonging to the core according to the standard single-layer method. Blue and small nodes code for the ROIs in the periphery. Links are yellow and thick if they connect two ROIs in the core, while they are blue and thin if they connect two peripheral nodes. Panel b) ROIs are ranked from top to bottom according to their richness in the structural (left column), functional (right column) and multiplex network (central column). In each column, the labels in bold/normal font stand for the ROIs that are in the core/periphery. For the sake of simplicity, only ROIs that are at least in one core (structural, functional or multiplex) are listed in the three columns. Red/blue and thick/thin lines identify ROIs that go into the core/periphery according to the multiplex approach.

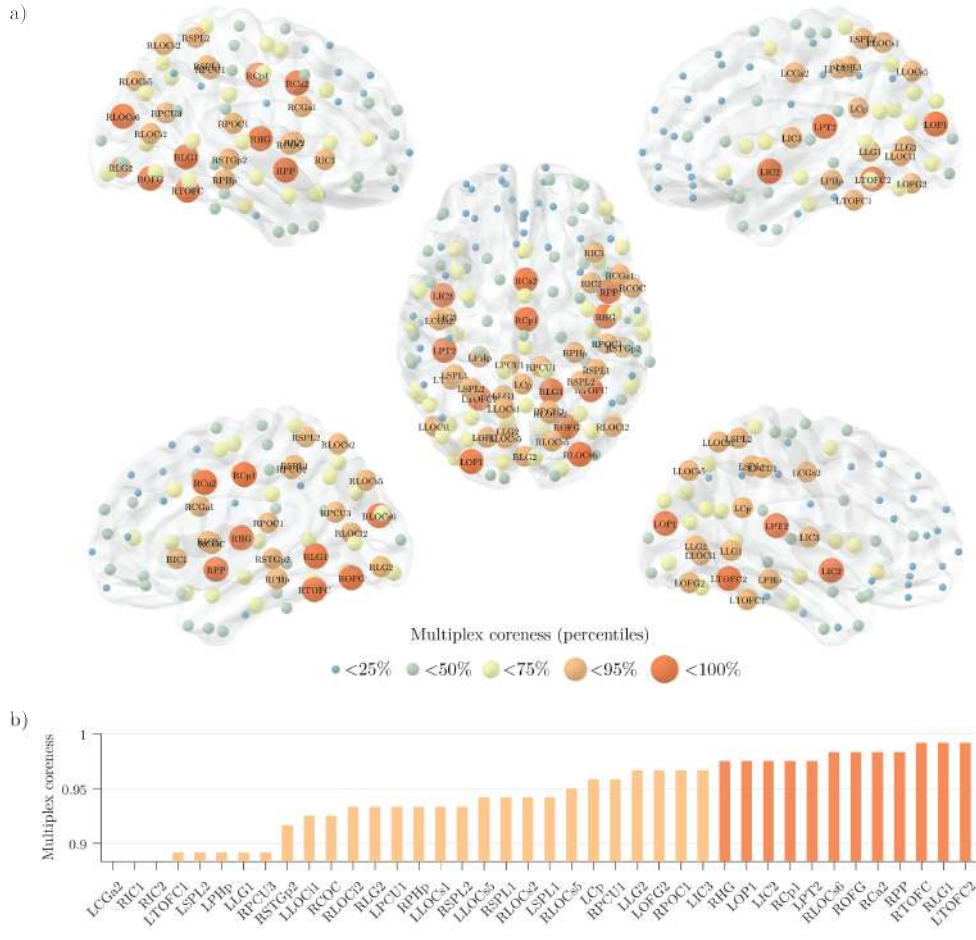


Figure 4: **The multiplex core of the human connectome.** Panel (a) shows the human brain, where regions of interest (ROIs) are highlighted based on their multiplex coreness. The color and size of the nodes are associated to the percentiles of multiplex coreness in each brain region, so that core nodes are larger in size and coloured in red. Left side shows the lateral view of the left hemisphere (top=dorsal, bottom=ventral). Right side shows the lateral view of the right hemisphere (top=dorsal, bottom=ventral). In the middle, the brain is shown from above, with the frontal lobe pointing upward. In panel (b) we report the ROIs corresponding to the 25% highest values of multiplex coreness. The color follows the same legend as in panel (a).

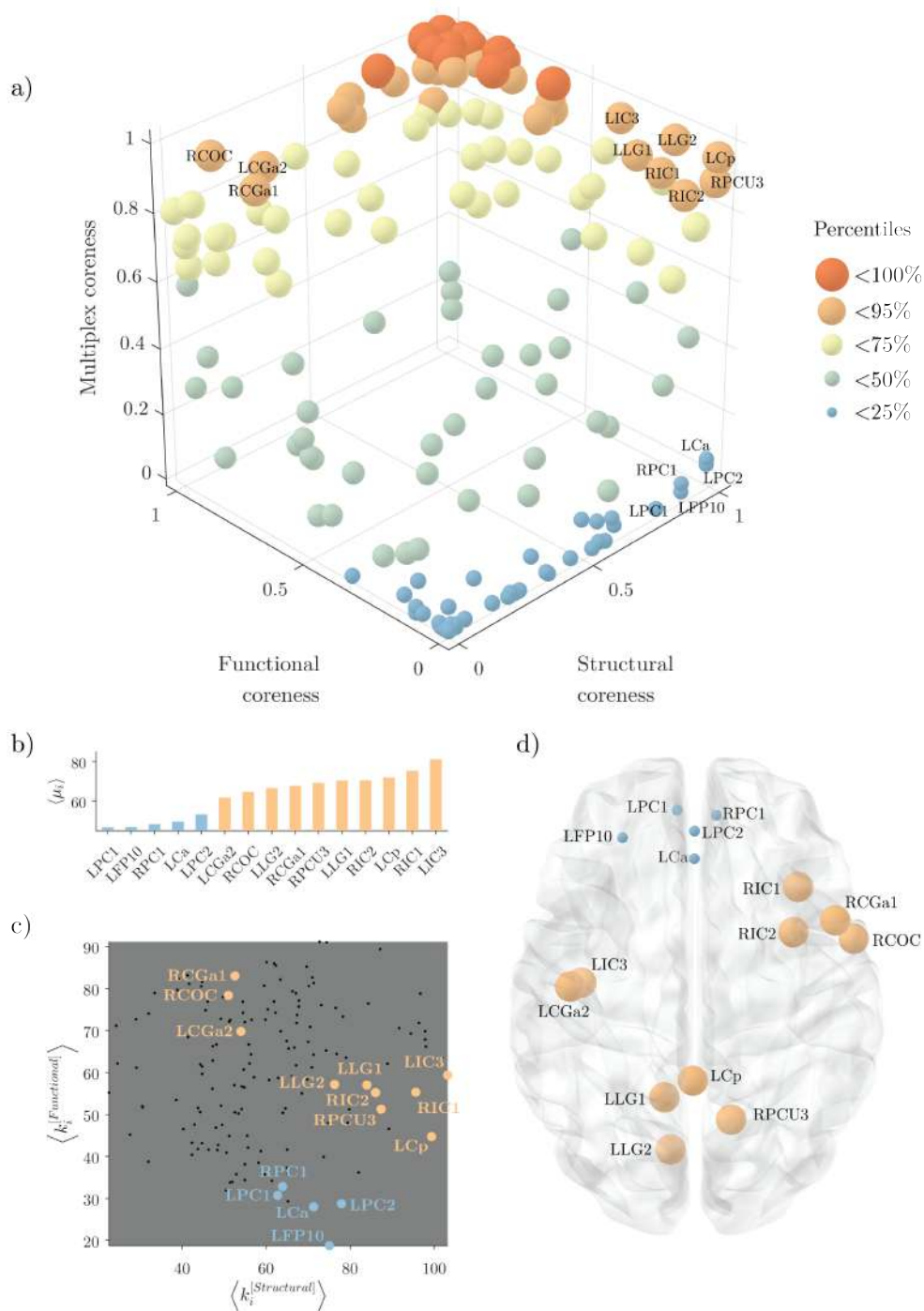


Figure 5: **Emergent non-trivial core regions in the multiplex brain.** Panel (a) shows the scatter plot of the structural, functional and multiplex coreness of the regions of interest (ROIs) in the brain. The color and size of the nodes are associated to the percentile of multiplex coreness across the set of brain regions, as in Fig. 4. Panel (b) reports the average value of multiplex richness $\langle \mu_i \rangle$ across the different thresholds for the ROIs with the strongest differences in structural and functional coreness. The color follows the same legend as in panel (a). Panel (c) illustrates the distribution of the ROIs (black points) as a function of their averaged structural and functional degree across all the thresholds. Only the ROIs listed in panel (b) are highlighted according to the same color legend as in panel (a).

569 ***S1. Robustness of the rich-core detection***

570 To test the robustness of our method, we have implemented a simulation model
 571 allowing random fluctuations in the distributions of values of the multiplex richness
 572 μ^+ . In particular, we have modified the value of each node i so that the new $\mu_i^+ =$
 573 $\mu_i^+ + \eta_i \mu_{i,\max}^+$. Here, $\mu_{i,\max}^+$ is the maximum value of the original richness and η_i
 574 is a random variable within the range $[-\eta_{\max}, \eta_{\max}]$, where η_{\max} is a tunable parameter
 575 ranging from 0 to 1. Hence, when $\eta_{\max} = 0$, the richness of the nodes is not altered;
 576 when $\eta_{\max} = 1$, the richness of the nodes is independently and maximally altered by a
 577 random factor within the range $[-\mu_{i,\max}^+, \mu_{i,\max}^+]$.
 578 We have applied this simulation model to the multiplex richness values of the brain
 579 networks illustrated in the Figure 3 of the main text and we have checked the composition
 580 (i.e., the size) of the core as a function of η_{\max} . Notably, for each value of η_{\max} we generate
 581 100 random samples. Results show that the average core size is relatively stable for a
 582 broad range of η_{\max} values (Fig. 1a). Notably, fluctuations are completely negligible
 583 until $\eta_{\max} = 0.04$, and have a high chance to significantly modify the identified rich core
 584 only when they are larger than 0.1 (Fig. 1b).

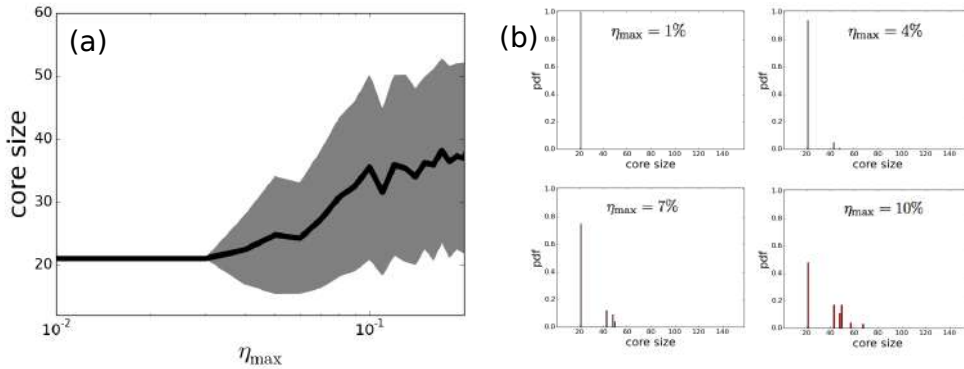


Figure 1: (a) Average core size in the multiplex brain network with $\langle k \rangle = 7$ as a function of the fluctuations parameter η_{\max} . (b) Cumulative density function of the core size for four selected values in the range $0.01 \leq \eta_{\max} \leq 0.1$.

585 Finally, we have compared the main results with those obtained through an alter-
 586 native approach where the core-periphery threshold is selected according to a statistical
 587 criterion. To this purpose, we have generated 100 degree-constrained random networks
 588 from both structural and brain networks. We have then normalized the actual μ^+
 589 values with respect to those obtained from the random samples according to a standard
 590 Z-score $z(\mu_i^+) = \frac{\mu_i^+ - \bar{\mu}^+}{\sigma(\mu^+)}$. We eventually report that the regional coreness (on which all
 591 the main results are based) is relatively stable regardless whether we have considered the
 592 maximum from the actual or normalized values of μ^+ (Fig. 2).

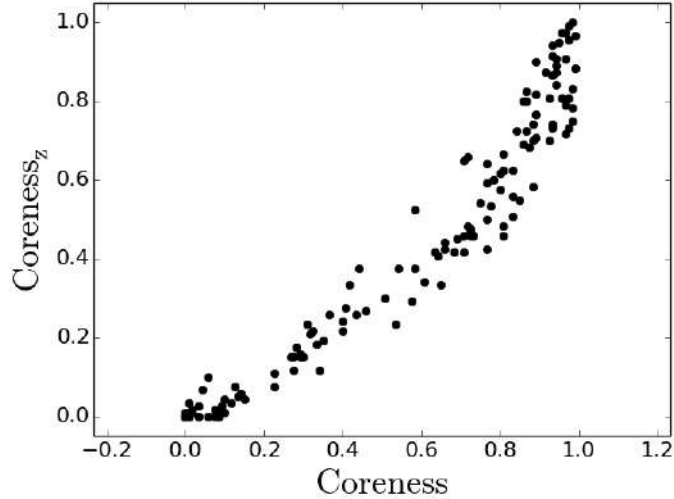


Figure 2: Scatterplot of the multiplex coreness obtained by looking at the maximum values of μ^+ and that obtained from the maximum of the corresponding Z-scores (Coreness z). The two measures are extremely correlated, $\rho_s = 0.97, p = 1.04 \times 10^{-80}$.

593 ***S2. Stochastic block model for rich cores in single-layer networks***

594 Suppose we have N nodes and we want to construct a single-layer network from which
 595 we can identify a partition into two sets: a core of size $N_c < N$ and a periphery of size
 596 $N_p = N - N_c$. Here we test the performance of the single-layer algorithm to detect rich
 597 cores [20] on a simple stochastic block model.

598 Let us consider N nodes from which N_c drawn at random are chosen to be part
 599 of the network core, whereas the remaining N_p are part of the periphery. A network
 600 with core-periphery structure is such that its adjacency matrix can be decomposed into
 601 four different blocks: a dense diagonal block encoding information on core-core links,
 602 a sparser diagonal block describing links among peripheral nodes, and two off-diagonal
 603 blocks encoding core-periphery edges.

604 In our block model, we connect two nodes with probability ρ_1 if they both belong to
 605 the core, with probability ρ_2 if one of them belongs to the core and one to the periphery,
 606 and with probability ρ_3 if they both belong to the periphery, $\rho_1 \geq \rho_2 \geq \rho_3$. Given a
 607 stochastic realization of the block model, we can extract the rich core of the network
 608 and compare it with the ground-truth, i.e. the set of nodes originally labeled as core
 609 nodes. In particular, we can test the accuracy of the algorithm for different choice of the
 610 parameters ρ_1, ρ_2 and ρ_3 .

611 Given the three probabilities, the expected total number of edges connecting two core
 612 nodes is $K_{cc} = \rho_1[(N_c - 1) * N_c/2]$, the expected total number of edges connecting two
 613 peripheral nodes is $K_{pp} = \rho_3[(N - N_c - 1)*(N - N_c)/2]$, and the expected total number of
 614 edges connecting a node in the core and a node in the periphery $K_{cp} = \rho_2[N_c * (N - N_c)]$.
 615 The total number of links is $K = K_{cc} + K_{cp} + K_{pp}$.

616 In the case $\rho_1 = \rho_2 = \rho_3 = \rho$ the nodes are statistically indistinguishable from a
617 structural point of view, the network lacks a core-periphery structure and specifying the
618 value of ρ simply sets the expected average degree of the network $\langle k \rangle = N\rho$. For instance,
619 for $N = 250$ and $\rho = 0.04$ we obtain $\langle k \rangle = 10$ and $K = 1250$. Of the different blocks of
620 the adjacency matrix, the exact value of the density of the block encoding links between
621 core and periphery nodes does not play a significant role [8]. For such a reason here we
622 set $\rho_2 = 0.04$, and study the core-periphery structure of the network as a function of
623 ρ_1 , with $\rho_1 > \rho_2$. The higher the value of ρ_1 , the stronger the core-periphery structure
624 of the system. In order to control for the density of the network, as we increases ρ_1 we
625 have to opportunely decrease the value of ρ_3 . The average degree $\langle k \rangle$ can be kept fixed
626 by setting

$$627 \quad \rho_3 = \frac{2}{(N_p) * (N_p - 1)} \left(K - K_{cc} - K_{cp} \right). \quad (1)$$

628 In our case with $N = 250$ and $\langle k \rangle = 10$, we have $K = 1250$ whereas K_{cc} and K_{cp}
629 are set once we fix the core size N_c and the value of ρ_1 . In Fig. 3 we show the average
630 Jaccard index J computed for the ground-truth partition and the partition extracted
631 by the algorithm on the stochastic realizations of the network as a function of different
632 values of ρ_1 for different core size.

633 As shown, J increases quickly until $\rho_1 = 0.2$ and only mildly after this point. This
634 indicates that $\rho_1 = 0.2$, corresponding to a value of $\rho_3 = 0.03$, can be considered as
635 the smallest density of the core-core block at which the core-periphery structure of the
636 network is sufficiently well-defined. For this reason, in the stochastic block model for
637 multiplex networks with different values of core similarity S_c described in Fig. 1 of the
638 main text, where we have $N = 250$ and $N_c = 50$ we set $\rho_1 = 0.2$.

639 Given the set of parameters ρ_1 , ρ_2 and ρ_3 we can also compute the average degree
640 $\langle k_c \rangle$ of core nodes

$$641 \quad \langle k_c \rangle = \rho_1(N_c - 1) + \rho_2(N_p), \quad (2)$$

642 the average degree $\langle k_p \rangle$ of the peripheral nodes

$$643 \quad \langle k_p \rangle = \rho_3(N_p - 1) + \rho_2(N_c). \quad (3)$$

644 so that we have

$$645 \quad \langle k \rangle = \frac{N_c \langle k_c \rangle + N_p \langle k_p \rangle}{N}. \quad (4)$$

646 In Fig. 4 we show the average Jaccard index J computed for the ground-truth partition
647 and the partition extracted by the algorithm as a function of $\langle k_c \rangle / \langle k_p \rangle$. **The Jaccard index**
648 **J is defined as**

$$649 \quad J = \frac{I_c^{[\alpha\beta]}}{N_c^{[\alpha]} + N_c^{[\beta]} - I_c^{[\alpha\beta]}}, \quad (5)$$

650 where $N_c^{[\alpha]}$ is the number of core nodes at layer α , $N_c^{[\beta]}$ is the number of core nodes at
651 layer β and $I_c^{[\alpha\beta]}$ is the number of nodes that are part of the core at both layers α and
652 β .

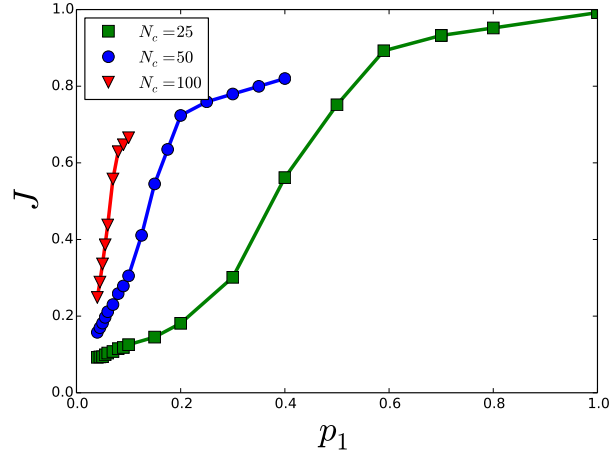


Figure 3: Jaccard index J for the groundtruth core-periphery partition and the partition obtained by the algorithm on realizations of the stochastic block model as a function of ρ_1 and for different core sizes N_c .

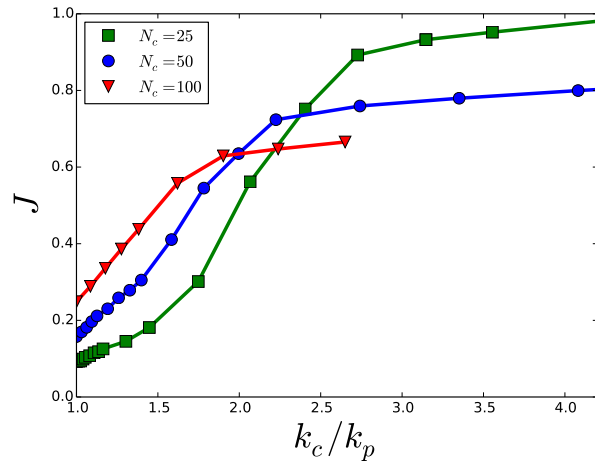


Figure 4: Jaccard index J for the ground-truth core-periphery partition and the partition obtained by the algorithm on realizations of the stochastic block model as a function of $\langle k_c \rangle / \langle k_p \rangle$ and for different core sizes N_c .

653 Supplementary figures

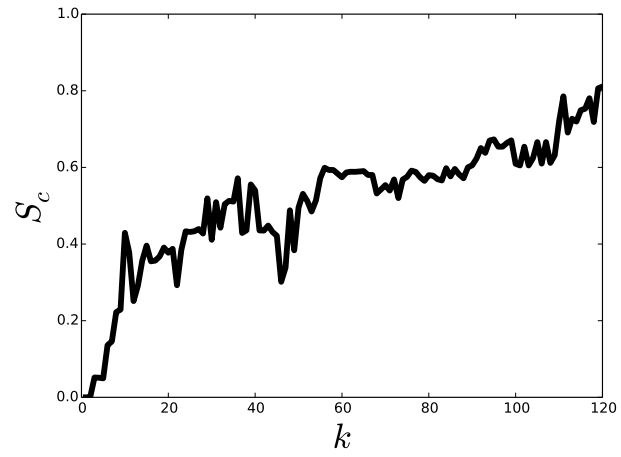


Figure S1: Core similarity S_c for the structural and functional brain networks thresholded at different values of average degree $\langle k \rangle$.

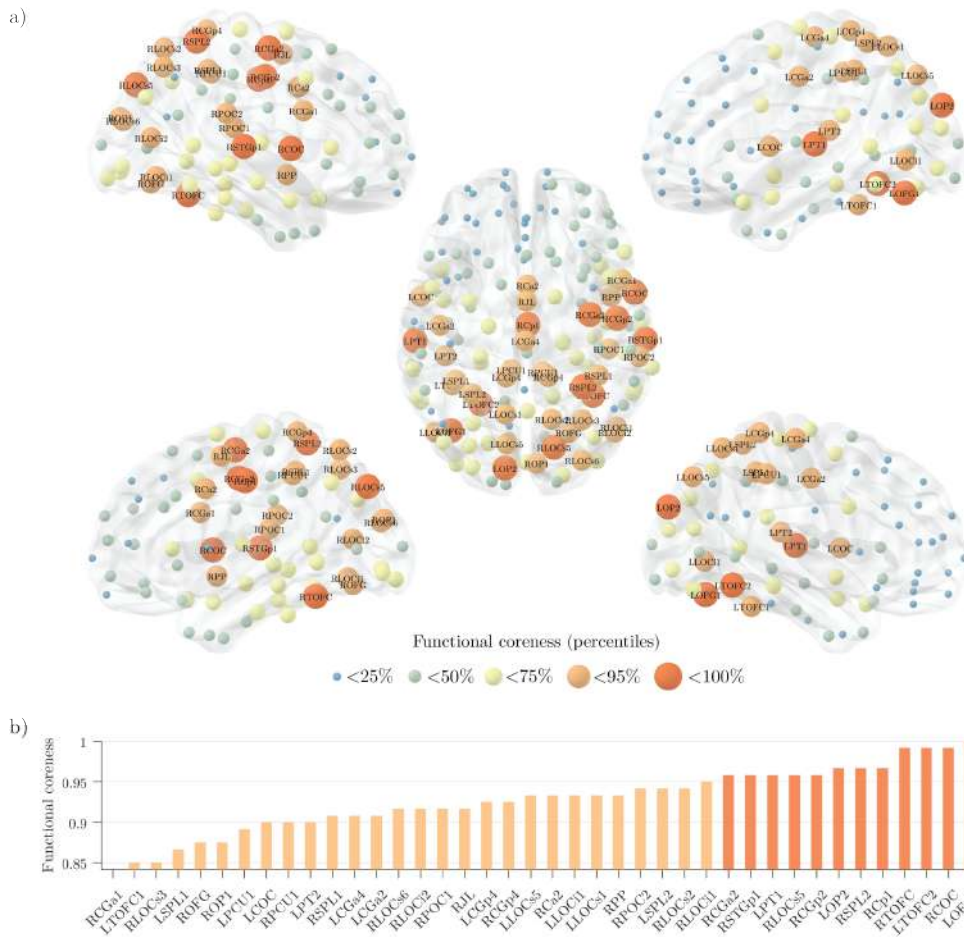


Figure S3: Panel a) shows the functional coreness from different points of view: external view in the top row, internal view in the bottom row. The color and size of each node code for the percentile to which it belongs as specified in the legend. In panel (b) we report the value of functional coreness for the nodes beyond the 75th percentile with the same color code.

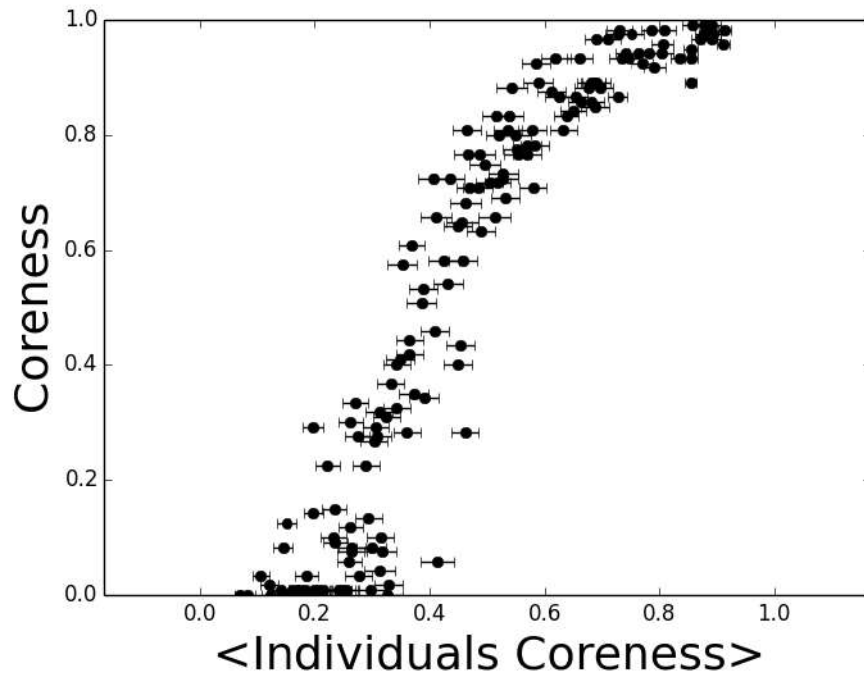


Figure S4: Coreness of the average as a function of average of the coreness. Each point corresponds to a brain region. On the y-axis we show the multiplex coreness of the group-averaged brain networks. On the x-axis we show the average of the multiplex coreness extracted from each individual. Error bars stand for standard error means. The corresponding Spearman's correlation coefficient is $\rho_s = 0.960$, $p = 2.72 \times 10^{-88}$.

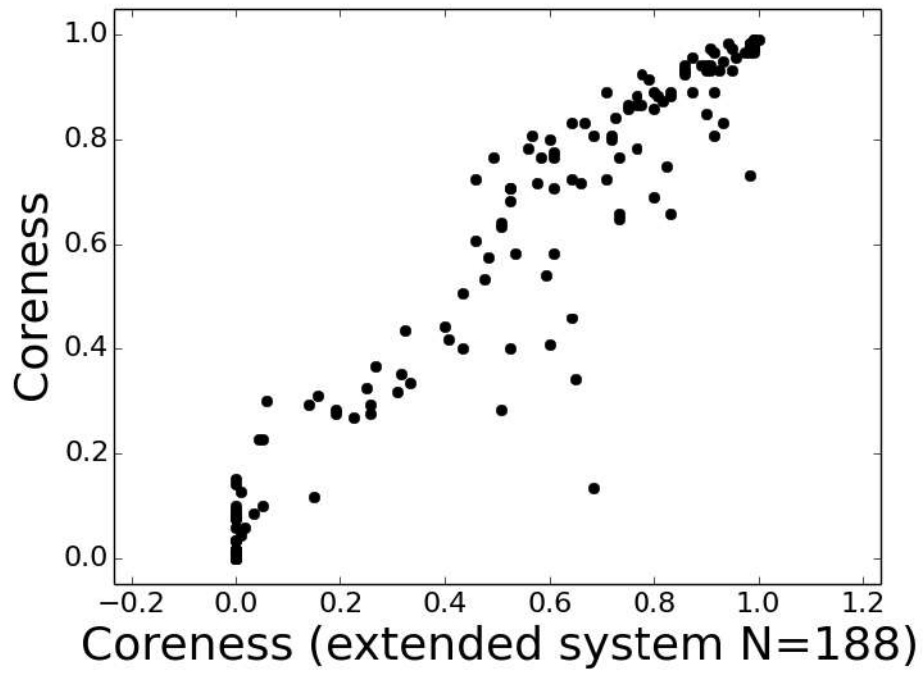


Figure S5: Scatterplot of the multiplex coreness of each ROI computed from brain networks with and without and without subcortical regions. The corresponding Spearman's correlation coefficient is $\rho_s = 0.95$, with a $p = 1.7 \times 10^{-78}$.

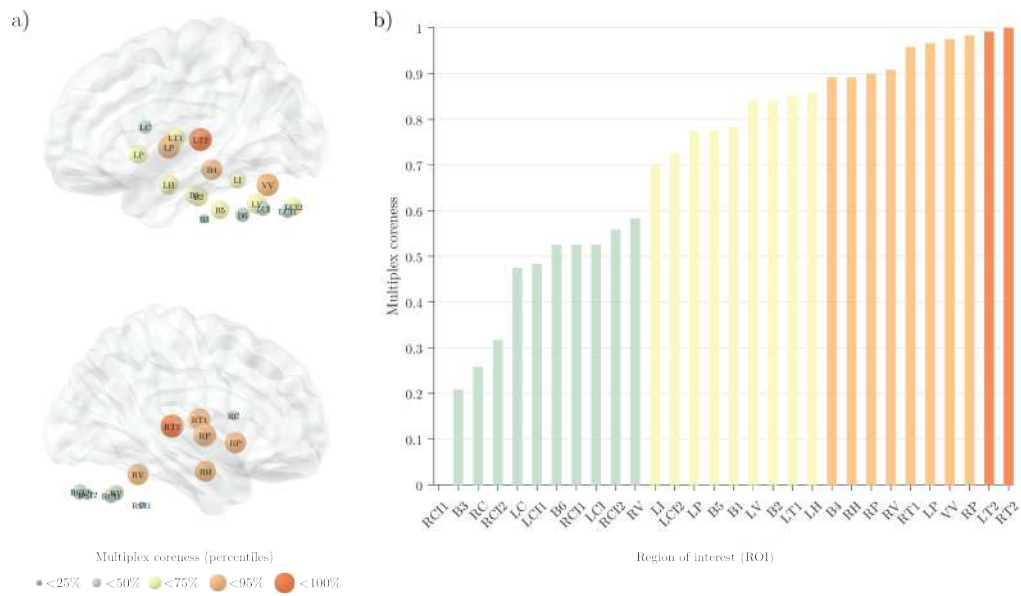


Figure S6: Panel a) shows the spatial position of the subcortical ROIs ($n = 38$). The size and color of the nodes code for the percentiles associated to their coreness with respect to all the ROIs ($n = 188$). Acronym : B = Brain stem; C = Caudate; CI = Crus; T = Thalamus; Pu = Putamen; Pa = Pallidum; V = Visual; H = Hippocampus. L = Left hemisphere; R = Right hemisphere; The number in the acronyms indicate the longitudinal position of ROIs. Panel b) shows the coreness of each subcortical ROI. The color codes for the percentile associated to their coreness with respect to all the other ROIs.

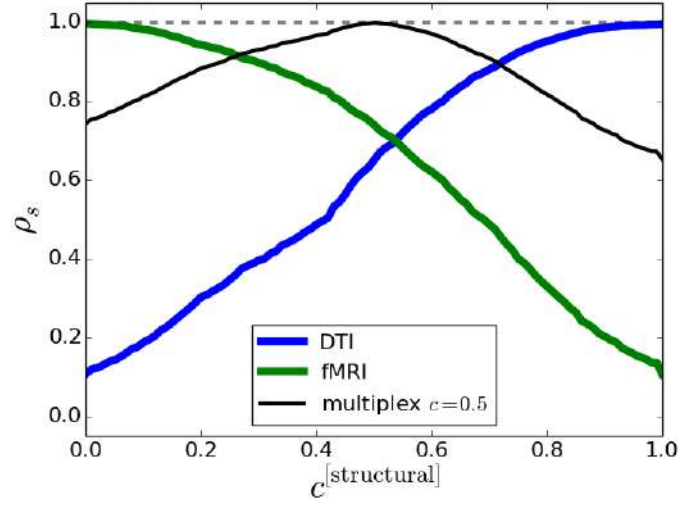


Figure S7: Sensitivity analysis for the multiplex brain coreness. We considered different coefficients $c^{[\alpha]}$ for the structural and functional layer. Specifically, $c^{\text{structural}} \in [0, 1]$ with $c^{\text{functional}} = 1 - c^{\text{structural}}$. We analyzed the similarity (in terms of Spearman correlation) between the unbiased multiplex coreness and the structural (DTI), functional (fMRI) and multiplex coreness as a function of $c^{\text{structural}}$. The multiplex coreness is relatively stable across different coefficients around the unbiased case $c^{\text{structural}} = c^{\text{functional}} = 0.5$ (black curve); In addition, $c^{\text{structural}} = 0.5$ leads to a multiplex coreness which is slightly more similar to the functional coreness (green curve), highlighting that the multiplex core is more than the sum of the cores at the different layers.

654 **Supplementary tables**

Layer	N_c
1	17
2	17
3	12
Multiplex	12

Layer	Layer	I_C
1	2	6
1	3	5
2	3	6
Multiplex	1	10
Multiplex	2	8
Multiplex	3	7

Table S1: In the left table we report the size N_c of the cores of the three layers (mutual trust, common operations, exchanged communications) of the Top Noordin Terrorists network [34] and of the multiplex core shown in Fig. 1 of the main text. In the right table we report the number of common core nodes I_C belonging to the different pairs of layers. The network is characterized by a core similarity $S_c = 0.38$ ($S_c^{[1]} = 0.32$, $S_c^{[2]} = 0.35$, $S_c^{[3]} = 0.46$. See Eq. 3 in the main text). We also report the number of common core nodes for the multiplex and each layer.

ROI label	Abbrev.	ROI label	Abbrev.
Left Angular	LAG	Right Central Opercular	RCOC
Left Central Opercular	LCOC	Right Cingulate anterior 1	RCa1
Left Cingulate anterior	LCa	Right Cingulate anterior 2	RCa2
Left Cingulate posterior	LCp	Right Cingulate posterior 1	RCp1
Left Frontal Medial	LFMC	Right Cingulate posterior 2	RCp2
Left Frontal Orbital 1	LFOC1	Right Frontal Orbital	RFOC
Left Frontal Orbital 2	LFOC2	Right Frontal Pole 1	RFP1
Left Frontal Pole 1	LFP1	Right Frontal Pole 10	RFP10
Left Frontal Pole 10	LFP10	Right Frontal Pole 2	RFP2
Left Frontal Pole 2	LFP2	Right Frontal Pole 3	RFP3
Left Frontal Pole 3	LFP3	Right Frontal Pole 4	RFP4
Left Frontal Pole 4	LFP4	Right Frontal Pole 5	RFP5
Left Frontal Pole 5	LFP5	Right Frontal Pole 6	RFP6
Left Frontal Pole 6	LFP6	Right Frontal Pole 7	RFP7
Left Frontal Pole 7	LFP7	Right Frontal Pole 8	RFP8
Left Frontal Pole 8	LFP8	Right Frontal Pole 9	RFP9
Left Frontal Pole 9	LFP9	Right Heschls	RHG
Left Inferior Frontal pars triangularis	LIFGpt	Right Inferior Frontal pars triangularis	RIFGpt
Left Inferior Temporal posterior 1	LITGp1	Right Inferior Temporal posterior 1	RITGp1
Left Inferior Temporal posterior 2	LITGp2	Right Inferior Temporal posterior 2	RITGp2
Left Inferior Temporal occipital	LITGt	Right Inferior Temporal occipital	RITGt
Left Insular 1	LIC1	Right Insular 1	RIC1
Left Insular 2	LIC2	Right Insular 2	RIC2
Left Insular 3	LIC3	Right Intracalcarine	RICL
Left Lateral Occipital inferior 1	LLOCi1	Right Juxtapositional Lobule	RJL
Left Lateral Occipital inferior 2	LLOCi2	Right Lateral Occipital inferior 1	RLOCi1
Left Lateral Occipital superior 1	LLOCs1	Right Lateral Occipital inferior 2	RLOCi2
Left Lateral Occipital superior 2	LLOCs2	Right Lateral Occipital inferior 3	RLOCi3
Left Lateral Occipital superior 3	LLOCs3	Right Lateral Occipital superior 1	RLOCs1
Left Lateral Occipital superior 4	LLOCs4	Right Lateral Occipital superior 2	RLOCs2
Left Lateral Occipital superior 5	LLOCs5	Right Lateral Occipital superior 3	RLOCs3
Left Lateral Occipital superior 6	LLOCs6	Right Lateral Occipital superior 4	RLOCs4
Left Lingual 1	LLG1	Right Lateral Occipital superior 5	RLOCs5
Left Lingual 2	LLG2	Right Lateral Occipital superior 6	RLOCs6
Left Middle Frontal 1	LMFG1	Right Lingual 1	RLG1
Left Middle Frontal 2	LMFG2	Right Lingual 2	RLG2
Left Middle Frontal 3	LMFG3	Right Middle Frontal 1	RMFG1
Left Middle Temporal anterior	LMTGa	Right Middle Frontal 2	RMFG2
Left Middle Temporal posterior 1	LMTGp1	Right Middle Frontal 3	RMFG3
Left Middle Temporal posterior 2	LMTGp2	Right Middle Frontal 4	RMFG4
Left Middle Temporal occipital	LMTGt	Right Middle Temporal anterior	RMTGa
Left Occipital Fusiform 1	LOFG1	Right Middle Temporal posterior	RMTGp
Left Occipital Fusiform 2	LOFG2	Right Middle Temporal occipital 1	RMTGt1
Left Occipital Pole 1	LOP1	Right Middle Temporal occipital 2	RMTGt2
Left Occipital Pole 2	LOP2	Right Occipital Fusiform	ROFG
Left Occipital Pole 3	LOP3	Right Occipital Pole 1	ROP1
Left Occipital Pole 4	LOP4	Right Occipital Pole 2	ROP2
Left Paracingulate 1	LPC1	Right Occipital Pole 3	ROP3
Left Paracingulate 2	LPC2	Right Paracingulate 1	RPC1
Left Parahippocampal posterior	LPHp	Right Paracingulate 2	RPC2
Left Parietal Operculum	LPOC	Right Parahippocampal posterior	RPHp
Left Planum Temporale 1	LPT1	Right Parietal Operculum 1	RPOC1
Left Planum Temporale 2	LPT2	Right Parietal Operculum 2	RPOC2
Left Postcentral 1	LCGp1	Right Planum Polare	RPP
Left Postcentral 2	LCGp2	Right Postcentral 1	RCGp1
Left Postcentral 3	LCGp3	Right Postcentral 2	RCGp2
Left Postcentral 4	LCGp4	Right Postcentral 3	RCGp3
Left Precentral 1	LCGa1	Right Postcentral 4	RCGp4
Left Precentral 2	LCGa2	Right Precentral 1	RCGa1
Left Precentral 3	LCGa3	Right Precentral 2	RCGa2
Left Precentral 4	LCGa4	Right Precentral 3	RCGa3
Left Precuneus 1	LPCU1	Right Precuneus 1	RPCU1
Left Precuneus 2	LPCU2	Right Precuneus 2	RPCU2
Left Subcallosal	LSC	Right Precuneus 3	RPCU3
Left Superior Frontal 1	LSFG1	Right Superior Frontal 1	RSFG1
Left Superior Frontal 2	LSFG2	Right Superior Frontal 2	RSFG2
Left Superior Frontal 3	LSFG3	Right Superior Parietal Lobule 1	RSPL1
Left Superior Parietal Lobule 1	LSPL1	Right Superior Parietal Lobule 2	RSPL2
Left Superior Parietal Lobule 2	LSPL2	Right Superior Temporal posterior 1	RSTGp1
Left Supramarginal anterior	LSGa	Right Superior Temporal posterior 2	RSTGp2
Left Supramarginal posterior	LSMp	Right Supramarginal anterior	RSMa
Left Temporal Fusiform anterior	LTFCa	Right Supramarginal posterior	RSGp
Left Temporal Fusiform posterior	LTFCp	Right Temporal Fusiform anterior	RTFCa
Left Temporal Occipital Fusiform 1	LTOFC1	Right Temporal Fusiform posterior 1	RTFCp1
Left Temporal Occipital Fusiform 2	LTOFC2	Right Temporal Fusiform posterior 2	RTFCp2
Left Temporal Pole 1	LTP1	Right Temporal Occipital Fusiform	RTOFC
Left Temporal Pole 2	LTP2	Right Temporal Pole 1	RTP1
Left Temporal Pole 3	LTP3	Right Temporal Pole 2	RTP2
Right Angular	RAG	Right Temporal Pole 3	RTP3

Table S2: Full list of Regions of Interest (ROIs) and abbreviations. Numbers denote the relative position within a macro area, i.e. higher values stand for more posterior ROIs.